Appendix Figures and Appendix Supplementary Methods:

Phosphorylation of FUS low-complexity domain disrupts phase separation, aggregation, and toxicity

[1]Zachary Monahan*, [2]Veronica H. Ryan*, [3]Abigail M. Janke, [3]Kathleen A. Burke, [1]Shannon N. Rhoads, [4]Gül H. Zerze, [5]Robert O'Meally, [4]Gregory L. Dignon, [6]Alexander E. Conicella, [7]Wenwei Zheng, [7]Robert B. Best, [5]Robert N. Cole, [4]Jeetain Mittal, [1]Frank Shewmaker, and [2,3,6]Nicolas L. Fawzi

[1]Department of Pharmacology and Molecular Therapeutics, Uniformed Services University, Bethesda, Maryland 20895, United States
[2]Neuroscience Graduate Program,[3]Department of Molecular Pharmacology, Physiology, and Biotechnology, and [6]Graduate Program in Molecular Biology, Cell Biology and Biochemistry, Brown University, Providence, Rhode Island 02912, United States
[4]Department of Chemical and Biomolecular Engineering, Lehigh University, Bethlehem, PA 18015, USA
[5]Johns Hopkins Mass Spectrometry and Proteomic Facility, Johns Hopkins University, Baltimore, Maryland 21218, USA
[7]Laboratory of Chemical Physics, National Institutes of Health, Bethesda, MD 20892, USA
*Z.M. and V.H.R. contributed equally as "co-first" authors

Corresponding authors:
Frank Shewmaker, C2125, 4301 Jones Bridge Road, Bethesda, Maryland 20895, email: fshewmaker@usuhs.edu;
Nicolas L. Fawzi, Box G-E, Providence, Rhode Island 02912, email: Nicolas_Fawzi@brown.edu

Keywords: ribonucleoprotein granule, amyotrophic lateral sclerosis, frontotemporal dementia, prion, intrinsically disordered protein
Running title: FUS phosphorylation disrupts assembly

Table of Contents **Page number**

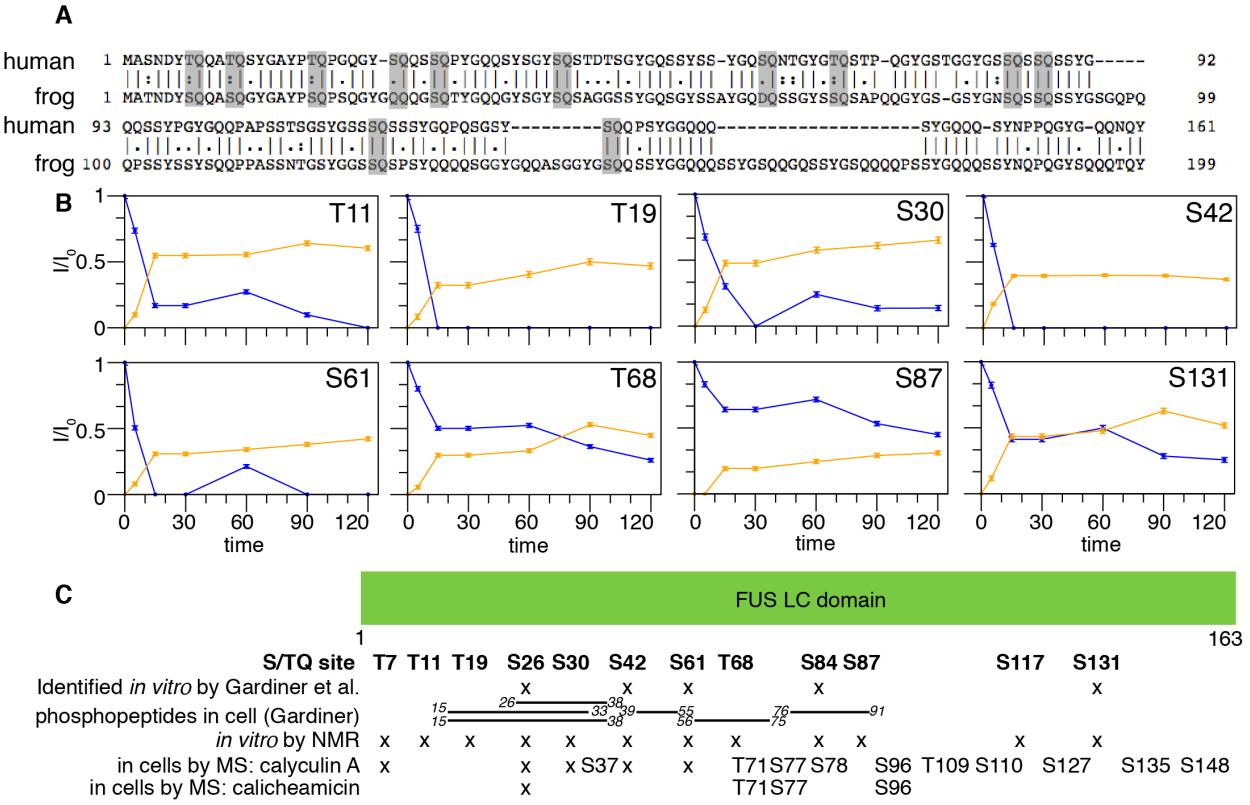

Appendix Figure S1: FUS is multiply phosphorylated *in vitro* and in cell (Related to Fig 1)

(**A**) FUS LC S/TQ sites (gray) are well conserved in vertebrates. Pairwise alignment (using EMBOSS Needle with default parameters) of the LC domain of FUS from human and *Xenopus laevis* (frog). Identical residues are indicated with vertical bars, conservative substitutions are indicated with dots.

(B) Change in intensity of FUS LC resonances of phosphorylated (orange) and non-phosphorylated (blue) residues during two-hour phosphorylation by DNA-PK *in vitro*. Remaining residues are presented in Figure 1C.

(**C**) Summary of previously published evidence and results presented here for FUS LC phosphorylation, including NMR data and mass spectrometry results with calyculin A and calicheamicin. Previous work by Gardiner et al identified phosphopeptides derived from cells subjected to ionizing radiation (IR) but did not localize the phosphosite within the peptides. Additionally, those authors demonstrated S42 phosphorylation in cell culture after IR using a polyclonal antibody specific for pS42.

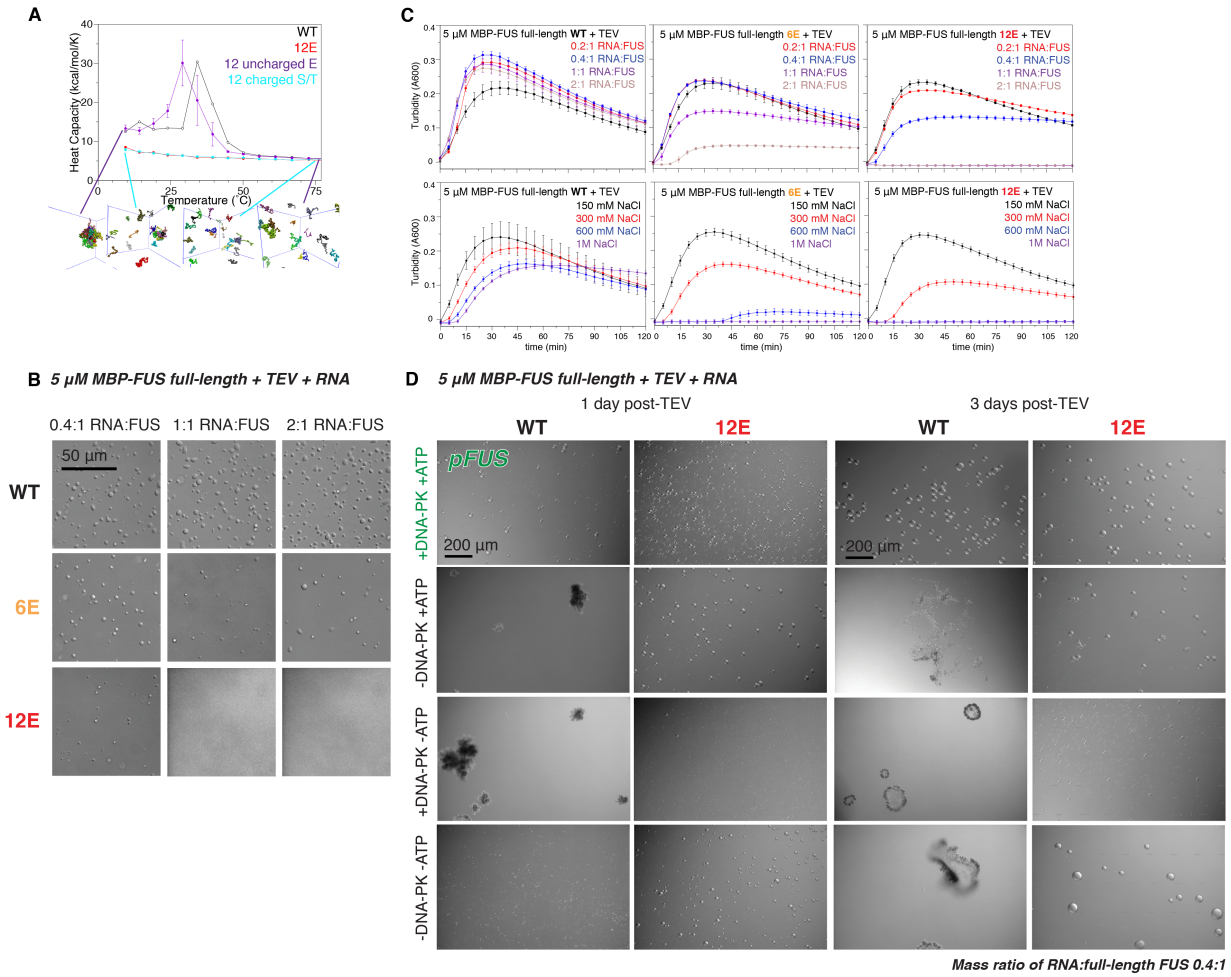

Appendix Figure S2: Mechanism of reduction in FUS phase separation by phosphomimetic substitution. (Related to Figure 2)

(**A**) Disruption of simulated FUS LC phase separation by phosphomimetic substitutions arises due to charge repulsion. Heat capacity curves and simulation snapshots for a variant with the wild-type sequence hydrophobicity terms but -1 net charge at S/TQ serine and threonine residues, charged S/T (blue line) does not show phase separation. A model incorporating a 0 net charge at E positions (purple line) shows phase separation albeit at a slightly lower temperature.

(**B**) DIC microscopy images of the conditions in Figure 2D show that 5 μM FUS FL 12E does not phase separate in the presence of 1:1 or 2:1 RNA:FUS FL by mass. The addition of 1:1 and 2:1 RNA:FUS FL by mass also reduces phase separation of 5 μM FUS FL 6E compared to that of 5 μM FUS FL WT. Images were taken 45 minutes after addition of TEV protease.

(**C**) Details of phase separation of full-length FUS (Figure 2C and 2D) as measured by turbidity at 600 nm. Addition of salt or RNA disrupts phase separation of phosphomimetic FUS much more than wild-type FUS. Reactions consisted of 5 μM full-length (FL) FUS WT, 6E, and 12E with increasing ratios of RNA:FUS FL by mass (top) or increasing salt concentration (bottom). Mean values +/- standard deviation of triplicate time-course experiments are plotted.

(**D**) Additional DIC microscopy images of full-length FUS WT and 12E following phosphorylation (row 1) and control (rows 2-4) treatments and 1 to 3 days of agitation at 25°C. Images shown here were taken with a 10x objective (see Figure 2F for 40x objective images) and verify aggregation of full-length FUS WT control treatments after 3 days of agitation at 25°C. Spherical assemblies of phosphorylated full-length FUS WT and full-length FUS 12E grow larger between time points, suggesting these assemblies fuse or undergo Ostwald ripening as monomers redistribute from smaller to larger droplets and LLPS persists.

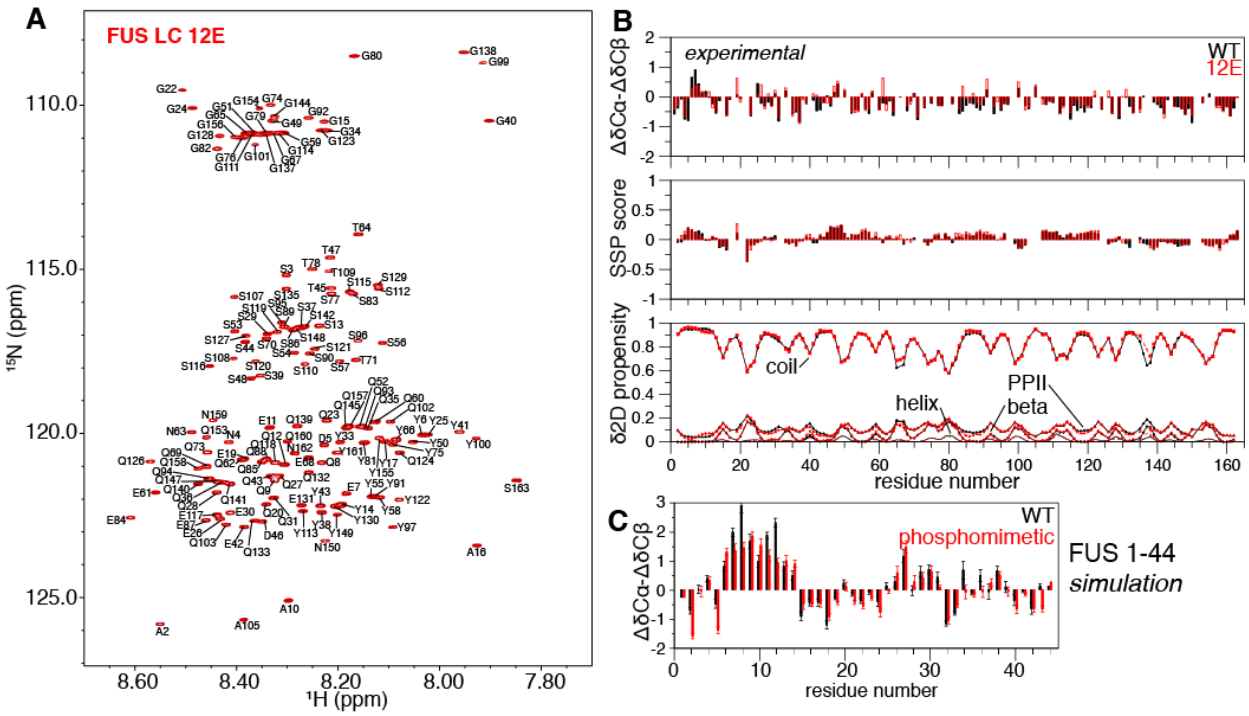

Appendix Figure S3: FUS LC WT and 12E are disordered as observed by NMR and MD simulation. (Related to Figure 3)

(**A**) The assigned two dimensional correlation spectrum (^{1}H ^{15}N HSQC) of FUS LC 12E remains similar to that observed for both wild-type and phosphorylated FUS LC (Figure 1B) and is consistent with structural disorder.

(**B**) The secondary structure population of FUS LC 12E is similar to wild-type and consistent with disorder. The difference in Cα and Cβ ^{13}C chemical shift deviations from a random coil reference (ΔδCα-ΔδCβ), secondary structure propensity (SSP), and predicted secondary structure population (δ2D) for FUS LC wild-type (black) and 12E (red) indicate structural disorder (ΔδCα-ΔδCβ and SSP near 0, δ2D predominantly coil). No notable structural differences are observed between wild-type and 12E, and both are consistent with disordered structure.

(**C**) ΔδCα-ΔδCβ calculated from the simulation of FUS 1-44 WT and phosphomimetic variant (incorporating EQ substitutions at all 6 S/TQ positions in FUS 1-44) indicate both simulated peptide ensembles lack stable structure and are predominantly disordered, though higher secondary structure propensity than observed by experiment for FUS LC is apparent from larger deviations from random coil values (y=0). These discrepancies may be due to differing peptide lengths (simulation: 45 residues; experiment 164 residues) but also underscore the difficulty in either in precisely capturing disordered low complexity domain structure by simulation or in empirical calculation of NMR chemical shift observables from simulation trajectories.

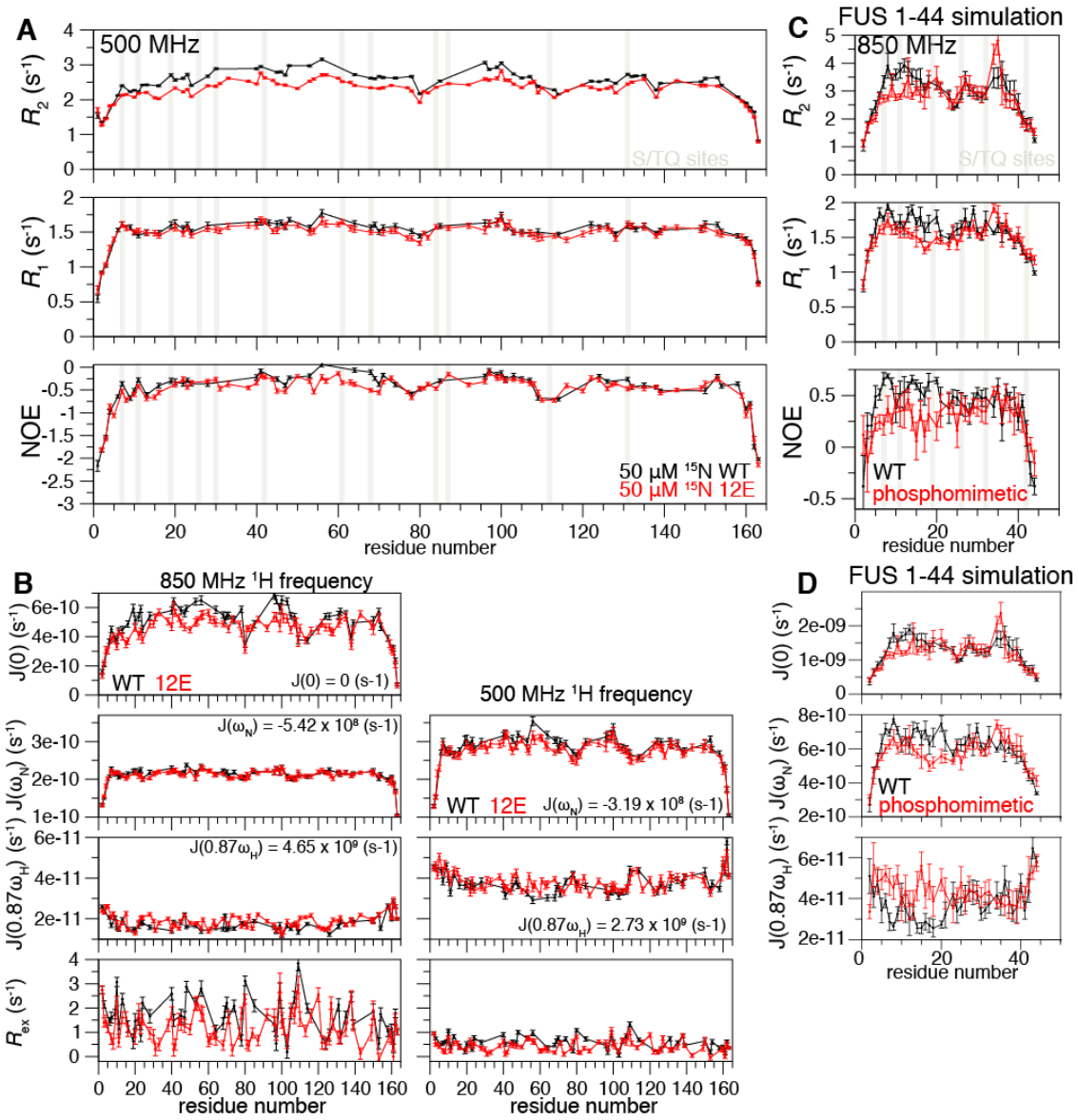

Appendix Figure S4: FUS LC wild-type and phosphomimetic spin relaxation differences can be explained by a combination of small differences in local motions and conformational exchange. (Related to Figure 3) (**A**) As observed at 850 MHz ^{1}H Larmor frequency, R_2, R_1, and NOE measured at 500 MHz ^{1}H Larmor frequency show small differences in local reorientational motions. (**B**) Reduced spectral density mapping showing J(0), J(ω_N), J(0.87ω_H), and fitted R_{ex} components at two fields. There is a small fitted R_{ex} component to the WT data that is not present in 12E, consistent with a contribution of conformational exchange. (**C**) R_2, R_1, and NOE (850 MHz ^{1}H Larmor frequency) calculated from an ensemble of simulation trajectories of FUS 1-44 indicate a slight dynamical difference between WT and the phosphomimetic variant. All six S/TQ sites present in 1-44 were replaced with EQ (FUS 1-44 phosphomimetic). (**D**) Reduced spectral density mapping predicted from the simulated FUS 1-44 showing J(0), J(ω_N), J(0.87ω_H) calculated for an 850 MHz ^{1}H Larmor frequency. Small differences in spectral density values between wild-type and phosphomimetic are consistent with slight differences in local reorientational motions.

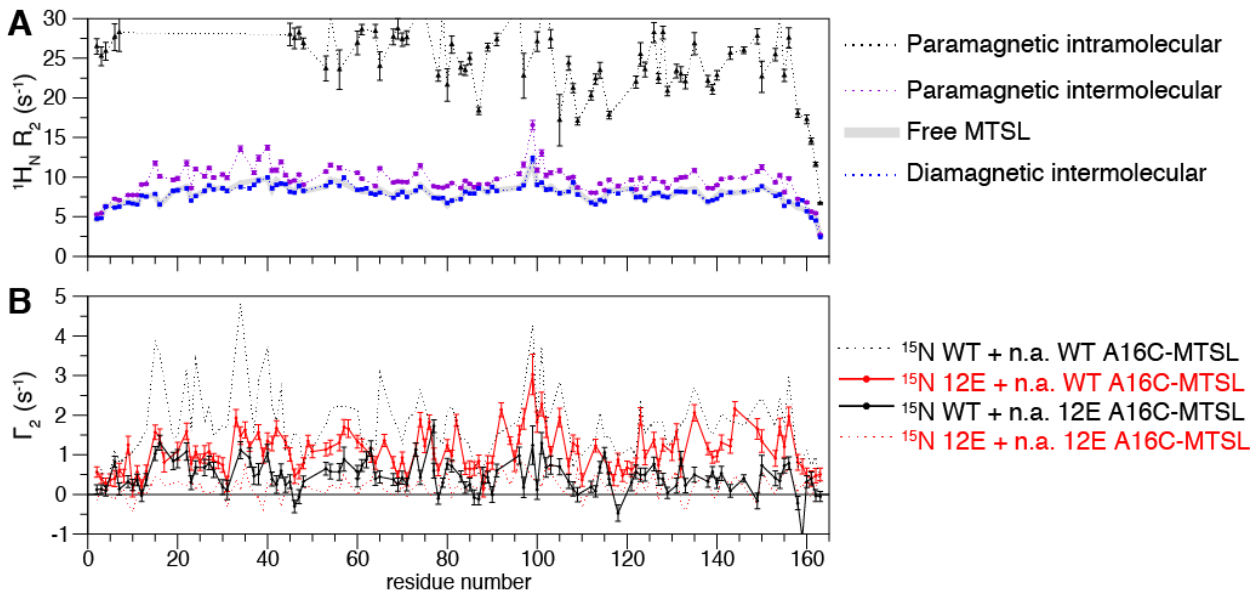

Appendix Figure S5: Transient interactions of FUS LC probed arise from LC:LC contacts and not due to non-specific interactions. (Related to Figure 3)

(**A**) Transverse relaxation values of backbone amide ^{1}H positions, ^1H_N R_2, (used to measure PREs) of 50 μM wild-type + 25 μM free (unconjugated) MTSL (Free MTSL, gray line) is the same as the diamagnetic control (blue dotted line). This equivalence in control experiments demonstrates that non-specific interactions between the peptide and MTSL are insufficient to generate the observed ^1H_N R_2 values used for calculation of intramolecular and intermolecular PREs (dotted black and purple lines, respectively, provided as examples of data used to calculate Γ_2 in Figure 3C and 3D).

(**B**) To confirm that differences between FUS LC wild-type and 12E intermolecular PRE values (Figure 3D) arise due to changes in intermolecular interaction ensembles, mixed intermolecular PRE experiments were conducted. Intermolecular PRE experiments were performed on ^{15}N FUS LC wild-type + natural abundance (n.a.) FUS LC 12E A16C-MTSL (black) and ^{15}N FUS 12E + n.a. wild-type A16C-MTSL (red). Both show Γ_2 values between the values for WT+WT and 12E+12E (black and red dotted lines, data reproduced from Figure 3D for clarity). These intermediate values indicate that the majority of the difference observed in Figure 3D is specifically due to differences in WT+WT and 12E+12E interactions.

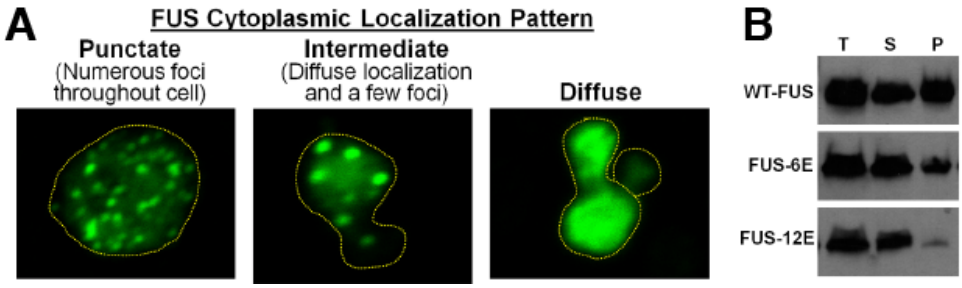

Appendix Figure S6: Phosphomimetic substitutions in the FUS's prion-like domain reduce its aggregation in yeast (Related to Figure 4).

(**A**) Representative aggregation patterns seen in yeast cells expressing FUS provided as references for scoring FUS cellular distribution in Figure 4B.

(**B**) Western blot (representative replicate) of yeast lysates shows phosphomimetic substitutions reduce the amount of FUS in the insoluble pellet. WT and variants of FUS were expressed from high-copy plasmids in strain W303 (T=total, S=supernatant, P=pellet). Samples derive from the same experiment and blots were processed in parallel.

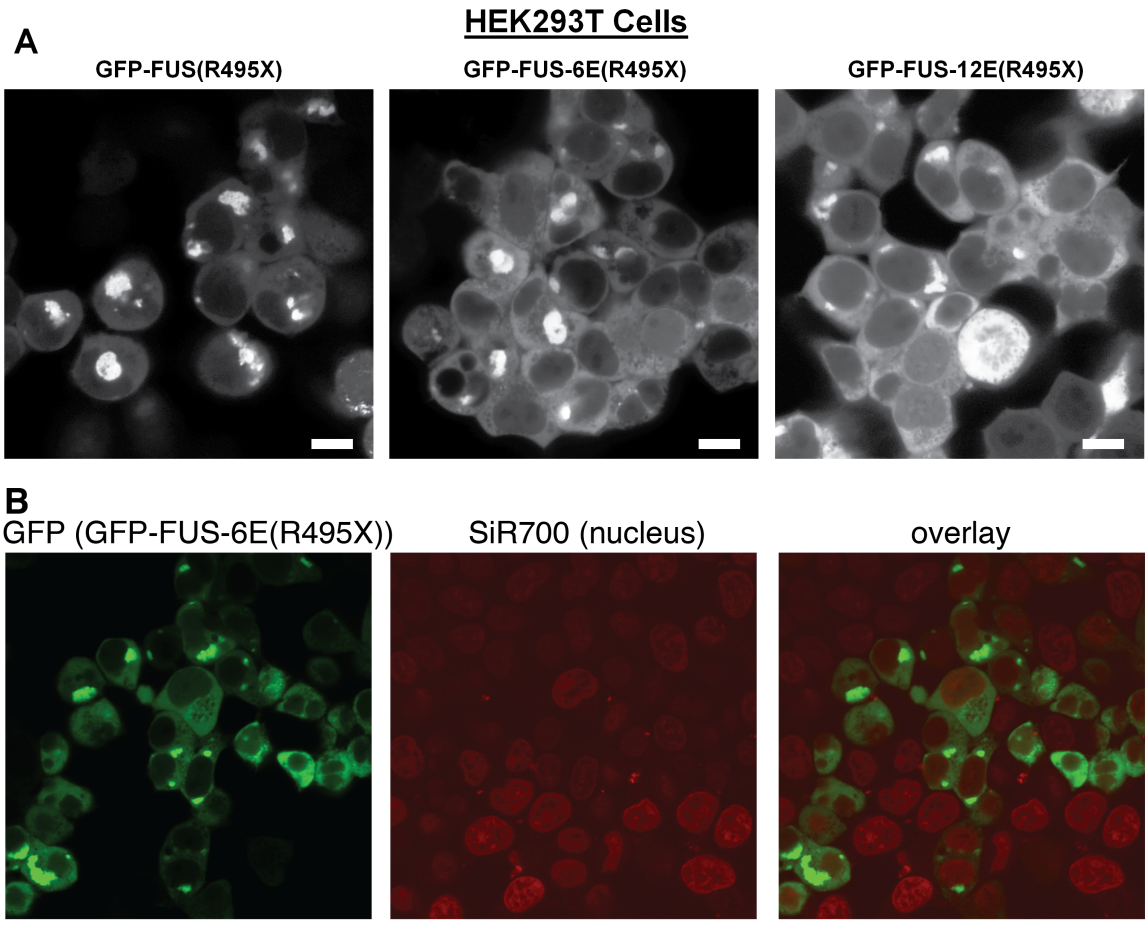

Appendix Figure S7: Both aggregated and diffuse forms of GFP-FUS(R495X) variants are in the cytoplasm of HEK293T cells (related to Figure 5).

(**A**) Image reproduced from Figure 5A but with enhanced brightness and altered contrast to show that all three GFP-FUS(R495X) variants (0E, left; 6E, center; 12E, right) are cytoplasmic and excluded from the nucleus (darker objects).

(**B**) Representative live image field of HEK293T cells transfected with GFP-FUS(R495X) 6E visualized by GFP fluorescence (left, green) and SiR700 nuclear stain (center, red) and overlay (right). Both the aggregated and diffuse forms of GFP-FUS(R495X) are cytoplasmic.

Appendix Supplemental METHODS

E. coli expressed recombinant protein for *in vitro* experiments

The following constructs were used for protein expression in BL21 Star (DE3) *E. coli* cultures (Life Technologies) is summarized here:

- FUS LC (1-163, untagged), inclusion body resuspended in pH 11 buffer, purified by HiTrapQ HP (anion exchanged) followed by Superdex 75 (gel filtration) (see Burke et al. 2015)
- MBP-FUS LC WT, purified from soluble fraction then subtracted in urea before Superdex75 in LC solubilizing buffer (20 mM pH 11 CAPS) (termed FUS LC WT after cleaving MBP)
- MBP-FUS LC 12E purified and substracted in native buffer and gel filtration in pH 11 CAPS
- MBP-FUS LC WT and 12E PRE variants incorporating A16C, S86C, or S142C mutations
- MBP-FUS FL WT, purified from soluble fraction and Superdex200 with MBP attached
- MBP-FUS FL 12E and 6E, purified from soluble fraction and Superdex200 with MBP attached
    - (MBP-FUS FL, in the pRP1B/THMT vector, gift of Rebecca Page, Brown University)

Expression

Uniformly ^{15}N labeled FUS LC, FUS LC WT, and FUS LC 12E, and PRE variants were expressed in M9 media with ^{15}N ammonium chloride as the sole nitrogen source. FUS LC WT and 12E PRE variants and MBP-FUS FL WT, 6E, and 12E were expressed in LB. Cell pellets of MBP-FUS LC were harvested from 1 liter cultures induced with 1 mM IPTG at OD600 0.7-1 after 4 hours at 37˚C. MBP-FUS FL cell pellets were harvested from 1 liter cultures induced with 0.5 mM IPTG at OD600 0.7-0.9 after 4 hours at 37˚C 200 rpm. LC pellets were resuspended in 20 mM sodium phosphate 300 mM sodium chloride 10 mM imidazole pH 7.4 and one EDTA-free protease inhibitor tablet. FL pellets were resuspended in 20 mM sodium phosphate 1 M sodium chloride 10 mM imidazole pH 7.4 and an EDTA-free protease inhibitor tablet. Resuspended pellets were lysed in an Emulsiflex C3 and the cell lysate cleared by centrifugation (20,000 xg for 60 minutes at 4˚C).

Purification

Soluble MBP-FUS FL WT, 6E, and 12E cell lysates were filtered with a 0.2 µm filter and loaded onto a HisTrap HP 5 mL column. Protein was eluted using a gradient of 10 to 300 mM imidazole. Fractions containing MBP-FUS FL were pooled, concentrated to 12 mL if necessary, and loaded onto a Superdex 200 sizing column equilibrated in 20 mM sodium phosphate 1 M sodium chloride pH 7.4. MBP-FUS FL WT, 6E, and 12E fractions determined by gel to contain minimal degradation products were pooled and concentrated separately in 20 mM sodium phosphate 1 M sodium chloride pH 7.4 up to 500 µM (50 mg/mL) using centrifugal filtration with a 10 kDa cutoff (Amicon, Millipore). MBP-FUS FL WT, 6E, and 12E protein were then flash frozen in 25% glycerol.

FUS LC purification was performed as in Burke et al. 2015. In short, inclusion bodies were resuspended in 20 mM CAPS pH 11 and resuspension cleared by centrifugation (20,000 xg for 60 minutes at 4˚C). The supernatant was filtered with a 0.2 µm syringe filter and loaded

onto a Q column in 20 mM CAPS pH 11. Protein was eluted with a gradient of 0 to 1 M NaCl. Protein was then applied to a Superdex 75/600 pg column equilibrated in 20 mM CAPS 150 mM NaCl pH 11. Fractions containing FUS LC were collected, concentrated, and buffer exchanged into 20 mM CAPS pH 11 by centrifugal filtration with a 3 kDa cutoff (Amicon, Millipore) to approximately 2 mM and flash frozen.

MBP-FUS LC WT and 12E (as well as corresponding PRE variants) cell lysates were filtered by syringe filtration using a 0.2 µm filter and loaded onto two HisTrap HP 5 mL columns in series. Protein was eluted using a gradient of 10 to 300 mM imidazole. Fractions containing protein, as determined by gel, were pooled and incubated with TEV protease overnight at room temperature. 12E constructs were then diluted to a final imidazole concentration of 40 mM, filtered, and loaded onto two HisTrap HP 5mL columns in series. WT constructs were solubilized with solid urea to 8 M, diluted to imidazole concentrations of 40 mM, filtered, and loaded onto two HisTrap HP 5mL columns in series. Flow through containing cleaved FUS LC was collected, concentrated to < 1 mL and diluted into 20 mM CAPS 150 mM NaCl pH 11 to a final volume of about 10 mL. Protein was then applied to a Superdex 75/600 pg column equilibrated in 20 mM CAPS 150 mM NaCl pH 11. Fractions containing protein were collected, concentrated, and buffer exchanged into 20 mM CAPS pH 11 by centrifugal filtration with a 3 kDa cutoff (Amicon, Millipore) to approximately 2 mM and flash frozen.

MTSL labeling: Single cysteine containing variants were stored in CAPS with 1 mM DTT. Prior to conjugating the label, stocks were diluted into 8 M urea, 20 mM HEPES pH 8 and desalted on a HiPrep 26/10 Desalting column (GE) to remove DTT. Protein was then incubated with 1 mM MTSL label (more than 10x excess) for 1 hour at room temperature. Protein was then desalted to remove excess label. Labeled protein was then concentrated and buffer exchanged into 20 mM CAPS pH 11 using centrifugal filtration with a 3 kDa cutoff (Amicon, Millipore) to about 2 mM and flash frozen.

Full-length FUS phase separation assays

MBP-FUS full-length WT, 6E, and 12E protein stored in 75% pH 7.4 20 mM sodium phosphate 1M NaCl and 25% glycerol at -80˚C was thawed on ice. After thawing, protein samples were centrifuged (17,000xg or 20,080xg for 5 minutes at 25˚C) to remove any precipitate and sample concentrations were confirmed by measuring absorbance at 280 nm and using extinction coefficients calculated by ProtParam (Wilkins et al., 1999). We report that freezing in 25% glycerol and/or [NaCl] ≥ 300 mM prevented any precipitation due to freezing. Protein stocks were kept at 25˚C during preparation of 96-well plate samples or microscopy samples.

Plate reader experiments: To assess the effect of increasing salt concentration on phase separation, MBP-FUS FL WT, 6E, and 12E were then diluted into pH 7.5 20 mM Tris buffers of varying salt concentrations such that the final NaCl concentration was 150, 300, 600, or 1000 mM and the final MBP-FUS full-length concentration was 5 µM (0.5 mg/mL). 5 µL of TEV protease (stored at 0.3 mg/mL in 50 mM Tris pH 7.5, 1 mM EDTA, 5 mM DTT, 50% glycerol, 0.1% Triton-X-100) or TEV protease storage buffer was added to create samples with final volumes of 100 µL in 96-well clear plates (Costar®) sealed with clear optical adhesive film (MicroAmp®, ThermoFisher). Turbidity measurements were recorded by measuring the optical density at 600 nm using a SpectraMax® M5 Microplate Reader (Molecular Devices) at 5 minute time intervals up to 2 hours after the addition of TEV protease (or TEV protease storage buffer as negative control). The microplate reader pre-mixed samples 5 seconds before beginning the

kinetic experiment, mixed 3 seconds between readings, and read from the bottom of the plate. Experiments were conducted in triplicate and then averaged. Turbidity values were reported after subtracting the average optical density of Tris buffer at 600 nm at each time point.

To assess the effect of RNA on FUS full-length WT, 6E, and 12E phase separation, MBP-FUS full-length was diluted to a final concentration of 5 μM (0.5 mg/mL) in pH 7.4 20 mM Tris 150 mM NaCl. Torula yeast RNA extract was dissolved at 10 mg/mL in pH 7.4 20 mM Tris 150 mM NaCl on ice. Dissolved RNA was then centrifuged at 12,000 rpm for 5 minutes at 4˚C. 260 μL of the supernatant was extracted and desalted into pH 7.4 20 mM Tris 150 mM NaCl using two 0.5 mL 7000 MWCO spin desalting columns (Zeba, ThermoFisher). Desalted RNA was quantified by UV (A260) and was generally recovered at a concentration of roughly 6 mg/mL. Desalted RNA was then added at 0.05 mg/mL, 0.1 mg/mL, 0.27 mg/mL, or 0.5 mg/mL to 0.5 mg/mL samples of MBP-FUS full-length WT or 12E such that the final mass ratios of RNA:cleaved FUS full-length protein were 0.2:1, 0.4:1, 1:1, and 2:1. Turbidity measurements were recorded using the same approach as above.

Differential interference contrast (DIC) microscopy: Morphological changes to full-length FUS WT, 6E, and 12E were observed with differential interference contrast on an Axiovert 200M microscope (Zeiss). TEV protease was added at a final concentration of 0.015 mg/mL to stocks of 5 μM MBP-FUS FL WT, 6E, and 12E. For short-term assays (< 2 hours, Figure S2B) designed to observe RNA-dependent differences in FUS full-length WT, 6E, and 12E aggregation, 0.1 mg/mL, 0.27 mg/mL, or 0.5 mg/mL desalted torula yeast RNA extract was added to 0.5 mg/mL samples of MBP-FUS full-length WT, 6E, or 12E such that the final mass ratios of RNA:cleaved FUS full-length protein were 0.4:1, 1:1, and 2:1. For all long-term assays (Figures 2E, 2F), desalted RNA was added at a final concentration of 0.1 mg/mL (mass ratio of 0.4:1 RNA: cleaved full-length FUS). RNA was desalted into pH 7.4 20 mM Tris 150 mM NaCl as described above. Protein samples were incubated in sealed plastic microcentrifuge tubes (USA Scientific Seal-Rite) with or without agitation (1200 rpm, Eppendorf Thermomixer) at 25˚C and morphological changes to FUS full-length WT, 6E, and 12E were observed up to 3 days after addition of TEV protease. 20 μL protein samples were placed on glass coverslips and imaged with a 10x, 20x or 40x objective. Note that for DNA-PK incubated samples (Figures 2F, S2D), 1200 rpm agitation at 25˚C was initiated after 1 hour of DNA-PK/TEV protease incubation at 30˚C. See in vitro phosphorylation methods for additional details on DNA-PK phosphorylation of FUS FL.

Full-length FUS FRAP experiments:

For FRAP experiments of FUS FL, primary amines within MBP-FUS FL were conjugated to DyLight 488 NHS Ester (Thermo Scientific) following manufacturer's instructions. Labeled MBP-FUS FL was then desalted twice serially with 0.5 mL 7000 MWCO spin desalting columns (Zeba, ThermoFisher) to ensure removal of all excess unconjugated dye. 1 μL of roughly 40 μM labeled MBP-FUS FL and 2.5 μL of 0.3 mg/mL TEV protease were added to 47.5 μL samples of 5 μM unlabeled MBP-FUS FL diluted into pH 7.4 20 mM Tris 150 mM NaCl. A 20 μL sample was imaged on a glass coverslip 45 minutes post-TEV cleavage of the MBP solubility tag using the 40x objective of an LSM 710 confocal microscope (Zeiss).

In vitro phosphorylation

FUS LC was phosphorylated by DNA-PK (Promega) in 50 µL reactions as follows. FUS LC was diluted out of CAPS to a final reaction concentration of 120 µM, with 1X DNA-PK reaction buffer, activation buffer, 500 units of DNA-PK, and remaining volume 10 mM ATP. The reaction was allowed to proceed for 120 minutes (or shorter as indicated for time course) at 37˚C. Phosphorylation was quenched with 10 µL 30% acetic acid to a final volume of 60 µL. Samples for NMR were then diluted directly with 20 mM MES pH 5.5 10% $^{2}H_2O$ to final NMR sample volume of 500 µL.

FUS FL was phosphorylated by DNA-PK in 25 µL reactions as follows. MBP-FUS FL was diluted out of 75% pH 7.4 20 mM NaPi 1M NaCl, 25% glycerol to a final concentration of 20 µM with 1X DNA-PK reaction buffer, activation buffer, 250 units of DNA-PK, 1.25 µL of 0.3 mg/mL TEV protease and remaining volume 10 mM ATP such that the final concentration of ATP was 4 mM. For control samples without DNA-PK and/or ATP, 1X reaction buffer and/or MilliQ, respectively, were substituted. Samples were incubated with DNA-PK and TEV protease simultaneously because concurrent cleavage of the N-terminal MBP solubility improved efficiency of DNA-PK phosphorylation as verified by mass spectrometry. Samples were incubated for 1 hour at 30˚C without agitation (for phosphorylation) and then diluted to 5 µM by adding 75 µL of pH 7.5 20 mM Tris 150 mM NaCl. Samples were then aliquoted in microcentrifuge tubes and incubated at 1200 rpm, 25˚C in an Eppendorf Thermomixer for up to 3 days and 20 µL samples were imaged with differential interference contrast on an Axiovert 200M microscope (Zeiss) microscope with 10X, 20X, and 40X objectives.

FUS LC microscopy

FUS LC was incubated for 2 hours at 37˚C in in vitro phosphorylation conditions. WT FUS was incubated with and without DNA-PK, while 12E was incubated without DNA-PK. Reaction was quenched with 10 µL 30% acetic acid. Reaction was then diluted by half into 50 mM MES 150 mM NaCl pH 5. 20 µL samples were spotted onto a coverslip and imaged using an Axiovert 200M microscope (Zeiss) with a 20x objective.

Solution NMR samples

FUS LC samples were created by diluting FUS LC from 20 mM CAPS pH 11 stock into 150 mM NaCl 50 mM MES pH 5.5 (pH adjusted with BisTris) including 10% $^{2}H_2O$ or 0 mM NaCl 20 mM MES pH 5.5 including 10% $^{2}H_2O$. Sample concentrations were estimated using the extinction coefficients calculated by ProtParam (Wilkins et al. 1999).

Solution NMR experiments

NMR experiments were recorded at 25˚C using Bruker Avance III HD NMR spectrometer operating at 850, or if indicated, 500, ^{1}H frequency equipped with a Bruker TCI z-axis gradient cryogenic probe. Experimental sweep widths, acquisition times, and the number of transients were optimized for the necessary resolution, experiment time, and signal to noise for each experiment type.

In vitro phosphorylation: *In vitro* phosphorylation was assessed by a series of ^{1}H-^{15}N HSQCs at 12 µM FUS LC diluted from the phosphorylation reactions. Each ^{1}H-^{15}N HSQC was acquired with 256* and 3072* complex pairs in the indirect ^{15}N and direct ^{1}H dimension with corresponding acquisition times of 74 ms and 172 ms, and sweep widths of 20 ppm and 10.5 ppm centered at 117 ppm and 4.7 ppm, respectively. Differences in peak intensity were quantified by the ratio of a peak intensity at a given time point to its corresponding peak intensity in a control sample with DNA-PK but lacking ATP (and thus is not phosphorylated) to account

for potential peak intensity attenuation or spectral changes by DNA-PK binding (no significant changes were observed). Error was calculated as standard deviation with error propagation.

Relaxation: Motions of the backbone of FUS LC in the dispersed/monomeric phase were probed using ^{15}N R_1, temperature-compensated ^{15}N R_2, and heteronuclear NOE experiments using standard pulse sequences (hsqct1etf3gpsitc3d, hsqct2etf3gpsitc3d, hsqcnoef3gpsi, respectively, from Topspin 3.2, Bruker). Interleaved experiments comprised 256*×3072* complex data pairs in the indirect ^{15}N and direct ^{1}H dimensions, respectively, with corresponding acquisition times of 78 ms and 172 ms, sweep width of 19 ppm and 10.5 ppm, centered at 117 ppm and 4.7 ppm, respectively. ^{15}N R_2 experiments had an interscan delay of 2.5 s, a Carr-Purcell-Meiboom-Gill (CPMG) field of 556 Hz, and total R_2 relaxation CMPG loop-lengths of 16.525 ms, 264.4 ms, 181.775 ms, 33.05 ms, 115.675 ms, 82.625 ms, and 165.25 ms. ^{15}N R_1 experiments had an interscan delay of 1.2 s, and total R_1 relaxation loop-lengths of 100 ms, 1000 ms, 200 ms, 800 ms, 300 ms, 600 ms, and 400 ms. Heteronuclear NOE experiments were conducted with an interscan delay of 5 s. Data were processed with nmrPipe (Delaglio et al., 1995), apodized with a cosine squared bell function in the ^{1}H dimension and a cosine bell function in the ^{15}N dimension. Best-fit R_2 relaxation rates were calculated using least squares optimization of $^{1}H/^{15}N$ peak intensities to a single exponential function.

Paramagnetic relaxation enhancement: Transient intra- and intermolecular interactions between monomers were probed using paramagnetic relaxation enhancement experiments. Backbone amide proton transverse relaxation rate constant, $^{1}H_N$ R_2, were measured (Fawzi et al., 2010) at 850 MHz ^{1}H frequency for paramagnetic and diamagnetic samples, with 256* and 3072* complex pairs in the ^{15}N indirect and ^{1}H direct dimensions, corresponding acquisition times of 74 ms and 172 ms, and sweep widths of 20 ppm and 10.5 ppm centered around 117 ppm and 4.7 ppm, respectively. Each $^{1}H_N$ R_2 experiment comprised six interleaved $^{1}H_N$ R_2 relaxation delays: 0.2 ms, 130.2 ms, 90.2 ms, 60.2 ms, 20.2 ms, and 40.2 ms. PRE values (Γ_2) were obtained from the difference in $^{1}H_N$ R_2 values for the paramagnetic and diamagnetic samples: $^{1}H_N$ R_2,para - $^{1}H_N$ R_2,dia.

Assignment experiments: Triple resonance assignment experiments were performed on samples of $^{13}C/^{15}N$ uniformly labeled FUS LC 12E (conditions: 20 mM MES final pH 5.5, 10% $^{2}H_2O$, 25°C) as described in Burke et al. 2015. CBCA(CO)NH, HNCACB, HNCO, HN(CA)CO, a high resolution HNCA, and HNN experiments with sweep widths 10 ppm in ^{1}H (center 4.7 ppm), 20 ppm in ^{15}N (center 117 ppm), 6.5 ppm (center 173 ppm) in ^{13}C for CO experiments, 55.95 ppm (center 41 ppm) in ^{13}C for CA/CB experiments, 22 ppm (center 51 ppm) for HNCA, and 20 ppm (center 116 ppm) in ^{13}C for HNN using standard Bruker Topspin3.2 pulse programs with default parameter sets (cbcaconhgp3d, hncagp3d, hncacbgp3d, hncacogp3d, hncogp3d, and hncannhgp3d, respectively).

Experiments comprised 84-100*, 250*, 91-120*, 50*, 3072-4096* complex data pairs in the indirect ^{15}N, indirect $^{13}C\alpha$, indirect $^{13}C\alpha/C\beta$, indirect ^{13}CO, and direct ^{1}H dimensions, respectively. Data were processed with nmrPipe using default linear prediction parameters for either constant time or real time indirect dimensions and assigned in CARA (Masse & Keller, 2005). Assignments were then transferred to 150 mM NaCl by NaCl titration – only very small shifts were observed. FUS LC WT assignments are from Burke et al. 2015, BMRB accession number 26672.

Reduced spectral density mapping

Discrete spectral density function values at frequencies 0, ω_N, and $0.870\omega_H$ were evaluated for ^{15}N spin relaxation data acquired at 850 MHz and 500 MHz ^1H Larmor frequencies using reduced spectral density mapping (Farrow et al., 1995), with the assumption that for high frequency (i.e. ω_H) terms either $J(\omega) \propto (1/\omega 2)$ or $J(0.87\omega_H) = J(0.921\omega_H) = J(0.955\omega_H)$, which were indistinguishable. Errors were estimated using a Monte Carlo procedure with 1000 simulated data sets.

Yeast strains, plasmids and media

Wild-type FUS and its phosphomimetic variants were subcloned from the described pET vectors into the multiple-cloning sites (MCS) of yeast expression plasmids pFPS425 (*CEN LEU2* P_{GAL1}) and pFPS426 (*2μ LEU2* P_{GAL1}) using NdeI/XhoI. The pFPS425 and pFPS426 plasmids are derivatives of previously described pH316 (Edskes & Wickner, 2002) and pH317 (Edskes & Wickner, 2000) possessing the following modified MCS: BamHI NdeI SacI XbaI XhoI [3xSTOP] PstI PvuII HindIII.

Yeast expression plasmids were transformed into strain W303 (MATa *leu2 ade2-1 ura3 can1 trp1 his3 gal*+) and grown in synthetic-complete glucose medium lacking leucine (SC-leu). To induce FUS expression, galactose was replaced as the carbon source (SCgal-leu). Qualitative growth assays were performed by spotting dilution series on solid SCgal-leu medium. Quantitative growth assays were performed in liquid SCgal-leu medium in 96-well plates. Growth at 30˚C was measured at 24 and 48 hours. Statistical analysis was performed with Prism statistical software (Graphpad), establishing a 95% confidence interval for the growth of each liquid culture.

Phosphomimetic substitutions for yeast assays

The following series of serine/threonine to glutamate substitutions were constructed in FUS expression vectors using site-directed mutagenesis: FUS-2E (19, 131), FUS-3E (26, 30, 68), FUS-4E (68, 84, 87, 117), FUS-6E (26, 30, 68, 84, 87, 117), FUS-9E (7, 11, 26, 30, 68, 84, 87, 117, 131), FUS-11E (7, 11, 19, 68, 26, 30, 42, 84, 87, 117, 131), FUS-12E (7, 11, 19, 68, 26, 30, 42, 61, 84, 87, 117, 131)

Mammalian cell culture and induction of intracellular FUS phosphorylation

HEK293T cells were maintained at 37˚C in polystyrene 75 cm^2 flasks or 24-well plates using Dulbecco's Modification of Eagle's Medium (DMEM) supplemented with 10% fetal bovine serum and 1 *x* Penicillin-Streptomycin-L-Glutamine (100 *x*, Corning Life Sciences, USA). To induce phosphorylation of FUS, calyculin A or calicheamicin were dissolved in DMSO, and subsequently added to cultures at concentrations ranging from 0.1 – 100 nM. DMSO without dissolved compounds was used as a control. Cells were treated for approximately 180 minutes before harvesting by scraping them from the bottom of the plates and then spinning them down (2k RPM, 4˚C, 2') using a table-top centrifuge and sterile centrifuge tubes. Cells were lysed by resuspension and incubation on ice for 30' in a derivative of RIPA buffer containing: 150 mM NaCl, 50 mM Tris-pH 8, 1% triton x-100, 0.1% SDS, 0.1% deoxycholate, 1% phosphatase inhibitor cocktail-3 (Sigma, USA), 1% Protease Inhibitor Cocktail with EDTA (Sigma, USA) and 1 mM phenylmethanesulfonyl fluoride (PMSF).

Western blotting

To generate lysates for determining if FUS phosphomimetic constructs were expressed at equivalent levels, yeast cells were mechanically disrupted with glass beads in non-denaturing yeast lysis buffer (50 mM Tris pH 7.5, 5 mM DTT, 50 mM NaCl, 5% glycerol, 5 mM EDTA, 1 mM

PMSF, one Pierce protease inhibitor tablet per 5 mL (Thermo Scientific)), and then spun at 10,000 rpm for 10' to generate a cleared lysate, followed by heating for 5 minutes at 99˚C in SDS-PAGE loading buffer. Samples were run at 100 V on any-kD (Bio-Rad) polyacrylamide gels and then transferred at 100 V to nitrocellulose membranes. Immunoblotting was performed with rabbit α-FUS monoclonal antibody (Bethyl, #293A) and HRP-conjugated α-rabbit antibody (Southern Biotech). Detection was performed using Supersignal West Pico Chemiluminescent Substrate (Thermo Scientific) and CL-Xposure film (Pierce/Life Technologies). Western blotting was performed as described above. Western blotting was similarly performed with lysates prepared from HEK293T cells, which were lysed as described above.

Lysate fractionation

To generate lysates for evaluating the propensity of phosphomimetic FUS to aggregate, yeast cells were mechanically disrupted with glass beads in non-denaturing yeast lysis buffer (50 mM Tris pH 7.5, 5 mM DTT, 50 mM NaCl, 5% glycerol, 5 mM EDTA, 1 mM PMSF, 1 Pierce protease inhibitor tablet per 5 mL (Thermo Scientific)), followed by two brief spins (3000 rpm, 3') to remove cellular debris and unbroken cells. The lysates were next spun at 10,000 rpm for 10' to generate pellet and supernatant fractions. Pellets were re-suspended in non-denaturing buffer to a volume equivalent to the supernatant volume. Western blotting was then performed as described above. Densitometry was performed using ImageJ software. Statistical analysis establishing 95% confidence was performed using Prism software (Graphpad). HEK293T cells were lysed as described above, and then spun at 2,000 RPM for 2' to remove debris and generate a total fraction. This fraction was then spun at 14,000 RPM for 20' to generate a supernatant and pellet fraction. Following supernatant removal, the pellet was resuspended to the same volume as the supernatant. Western blotting was performed as above.

Filter retardation assay

Yeast cells were mechanically disrupted in non-denaturing yeast lysis buffer as described for the lysate fractionation experiments, except Sigma Protease Inhibitor Cocktail was used instead of a Pierce Protease Inhibitor Tablet because it generates less insoluble debris that potentially limits the flow of lysate through a cellulose acetate membrane. The lysates were added to either a 1% SDS or SDS-free preparation of lysis buffer and mixed by pipetting. These solutions were vacuum filtered through a 0.2 μM cellulose acetate membrane and washed several times in the same buffer. The cellulose acetate was developed via Western blotting as described above.

Fluorescence microscopy

To visualize the aggregation of FUS in yeast cells, W303 cultures (with pZM5-FUS(WT), or pZM5-FUS(12E)) were grown in SC-leu medium overnight, and then protein expression was induced by switching the cells to SCgal-leu medium for an additional 16 hours. Approximately 2 x 10^8 cells were fixed for 30 minutes in 4% paraformaldehyde at room temperature, and then centrifuged for 3 minutes at 4000 rpm. Following re-suspension in 500 uL 1.2 M sorbitol buffered with 0.1 M potassium phosphate (pH 6.4), 1 uL of BME and 20 uL of 100T zymolyase (0.5 mg/mL) were added, and cells were incubated at 37˚C for 30 minutes. The resulting spheroplasts were spun at 500 rpm for 5 minutes, and re-suspended in 40 mM potassium phosphate buffer, pH 6.4. Cells were mounted on poly-L-lysine coated slides and probed with anti-FUS (Bethyl, #293A), washed, and probed with Alexa Fluor 488 goat anti-rabbit. The slides were coated with ProLong mounting medium with DAPI (Invitrogen) and visualized on a Zeiss Pascal Confocal Microscope and processed with ZEN 2012 software.

For quantifying FUS aggregation, five fields of each experimental group were obtained using ZEN 2012 software, and sets of arbitrarily selected cells were chosen from these fields. These cells were then characterized as having *diffuse*, *intermediate*, or *punctate* FUS expression patterns in their cytosol. Following categorization, these results were plotted on a frequency plot.

Mass Spectrometry

Samples for mass spectrometry were immunoprecipitated from HEK 293T cell lysate using the Dynabeads Protein G immunoprecipitation kit (Thermo Fisher, USA) following treatment with DMSO (Sigma, USA), calyculin A (Sigma, USA) or calicheamicin (Pfizer, USA) HEK 293T cells were seeded and grown to approximately 90% confluence in 24 well plates (Corning, USA) at conditions of 37˚C, 5% CO_2. Cells were then treated with 1% DMSO, 50 nM calyculin A, or 50 nM calicheamicin and incubated for approximately 3 hours at 37˚C.

Cells were subsequently scraped from the wells, pooled into microcentrifuge tubes (Eppendorf, Germany) by treatment condition, and pelleted by centrifugation at 3000 RPM, for 3 minutes. The resulting pellet was resuspended in modified RIPA lysis buffer (150 mM NaCl, 50 mM Tris pH 8.0, 1% Triton X-100, 0.1% sodium deoxycholate, 0.1% SDS, 1% mammalian cell protease inhibitor cocktail (Sigma, USA), 1% phosphatase inhibitor cocktail 3 (Sigma, USA), 1 mM PMSF (Thermo, USA)). Resuspended cells were incubated on ice for approximately 30 minutes with intermittent pipetting.

The protein lysate was subsequently cleared by 14,000 RPM centrifugation for 20 minutes at 4˚C. The cleared lysate was added to the magnetic Dynabeads, per manufacturer's instructions. Purified protein was eluted in 20 µL fractions of elution buffer, and frozen at -80˚C prior to analysis by LC/MS.

Analysis by LC/MS was carried out at the Johns Hopkins University Proteomics Core Facility (Baltimore, MD, USA), using trypsin and chymotrypsin digests and phosphopeptide enrichment to identify specific phosphorylation sites on immunoprecipitated FUS (Thingholm et al., 2006). Immunoprecipitated FUS samples were reduced with DTT and and alkylated with iodoacetamide before each was placed onto an Amicon (EMD Millipore) 30 kD filter previously washed three times with distilled water. The samples were spun at 14,000 xg for 3 minutes before adding 300 µL of 10mM triethylammonium bicarbonate (TEAB) and spinning for 3 minutes 2 more times. Two 20 µg vials of trypsin (Promega, Madison Wisconsin) were dissolved in 1 mL of 10 mM TEAB and 300 µL was added to each Amicon filter for overnight digestion at 37˚C. The following day the digested FUS peptides were spun at 14000 xg for 3 minutes with two 300 µL TEAB washes and set aside leaving the intact N-terminal LC domain still on the filter. Next, two 25 µg vials of chymotrypsin (Promega, Madison Wisconsin) were brought up in 1 mL of TEAB containing 10 mM CaCl2 and 300 µL was added to each Amicon filter for overnight digestion at 37˚C. The following day the filters were spun at 14,000 g and washed two times with 300 µL 10 mM TEAB. The filtrate containing the chymoptryptic digest of the N-terminus was then evaporated to dryness in a speedvac.

A titanium dioxide phosphopeptide enrichment protocol was used to enrich the phosphopeptides from the trypsin/chymotrypsin double digested peptides. Briefly the peptides were brought up in 80 µL of starting buffer consisting of 80% acetonitrile (ACN), 3.5% trifluoroacetic acid (TFA). 2 µL of the peptides in starting buffer were dried for non-enriched analysis. An enrichment solution containing 37.5 mg dihydroxybenzoic acid (DHB), 15 mg

titanium dioxide (TiO_2) 5 µm particle size and 1.5 mL of starting buffer was then vortexed for 2 hours to equilibrate the DHB with the TiO_2 beads, which assists in preventing nonspecific binding. 50 µL of the enrichment solution was carefully added to the remaining 80 µL of peptides such that the TiO_2 was suspended in the pipette tip uniformly. The mixture of peptides in starting buffer and enrichment buffer was then vortexed for another 2 hours. Next the suspension with peptides and TiO_2 was aliquoted onto a filter tip and spun at 2000 g leaving the TiO_2 with bound phosphopeptides on top of the filter. 75 µL of a wash buffer consisting of starting buffer plus 1 M glycolic acid was used to rinse the DHB from the sample 2 times followed by a final rinse buffer containing 80% ACN, 0.1% TFA as the last step before phosphopeptide elution. Phosphopeptide elution was performed using 50 µL of 30% ACN, 3% NH_4OH and collecting 3 rinses at 2000 g. The phosphopeptides eluted were then neutralized with 50 µL of 10% formic acid then evaporated to dryness in a speedvac.

The LC/MS/MS analysis was performed on a Q-Exactive Plus mass spectrometer with an EasyLC nano flow chromatography system (Thermo Scientific). The samples were trapped at 5µL/min then eluted onto a 20 cm x 75 µm i.d. C18 column for a 120 minute gradient at 300 nL/min. The mass spectrometer was set at 70,000 resolution for MS and 35,000 resolution for MS2 with target of 3e6 for MS and 1e5 for MS2. The intensity threshold was set at 3.3e4 with a loop count of top 15 precursors selected for MS2. Maximum injection times were set to 60 and 150 milliseconds respectively and a normalized collision energy of 28 was used. The data was searched against the RefSeq2015 Human database using PEAKS 7.0 (Bioinformatics Solutions) with variable oxidation of M, phosphorylation of STY, deamidation of NQ, and carbamidomethyl C. Mass tolerances were set to 8.0 ppm for precursor and 0.02 daltons for fragment ions. Peptides were filtered at the 1% FDR level.

Simulation Methods

We perform parallel tempering metadynamics in well-tempered ensembles (PTMetaD-WTE) simulations of wild type and phosphomimetic versions 1-44 fragment of FUS (FUS 1-44) in aqueous solution, using GROMACS-4.6.7 (Berendsen et al., 1995, Hess et al., 2008) and Plumed 2.2 (Bonomi et al., 2009). In standard parallel tempering simulations, a number of replicas of the system are simulated at different temperatures (Sugita & Okamoto, 1999). Exchanges between adjacent temperature replicas are attempted periodically and are accepted based on a Metropolis criterion. The enhanced sampling in standard parallel tempering simulations is achieved by periodic exchanges with high temperature replicas, which can overcome barriers in the potential energy landscape. However, the number of parallel simulation replicas required for sufficient energy overlap to generate efficient exchange increases rapidly with system size, needing many dozens of replicas for simulations of disordered proteins. To help overcome this problem, we combined metadynamics and parallel tempering as described previously (Bussi et al., 2006). Here, potential energy of the system is introduced as a collective variable to bias in a well-tempered metadynamics scheme (well-tempered ensemble or WTE) (Bonomi & Parrinello, 2010). WTE amplifies potential energy fluctuations maintaining the same average energy, thereby reducing the number of replicas necessary for a sufficient exchange acceptance percentage (Bonomi & Parrinello, 2010, Deighan et al., 2012). Here, sixteen replicas were used within a temperature range of 300-518 K and exchanges between adjacent replicas were attempted every 1 ps. Temperatures of the replicas were adjusted, initially based on geometric spacing between 300 K and 518 K, to obtain uniform acceptance probability (of

approximately 35%) between all adjacent replica pairs (Prakash et al., 2011). All the replicas were started from unstructured configurations of the peptides. For the first 50 ns of the run, WTE was turned on for all replicas, except the 300 K replica (Prakash et al., 2011, Sutto & Gervasio, 2013). During run extension, the energy bias accumulated in the first 50 ns is loaded as a static bias. 1.2 and 500 kJ/mol gaussian height and width were used, respectively, together with a deposition frequency of every 4 ps and a bias factor of 36. Peptides were simulated for 200 ns per replica, last 150 ns of 300 K replica for both peptides were analyzed as equilibrium structural ensemble. NMR chemical shift deviations and probability density function of radius of gyration are presented from these equilibrium structural ensembles of wild type and phosphomimetic versions of the FUS peptide. NMR chemical shift deviations in the equilibrium ensemble are calculated using an empirical chemical shift deviation prediction algorithm, SPARTA+ (Shen & Bax, 2010).

Amber ff99SBws protein force field (Best et al., 2014) was used in combination with TIP4P/2005 water model (Abascal & Vega, 2005) with optimized protein-water interactions to improve protein-protein interaction strengths and the size of unfolded and disordered peptides (Best et al., 2014). Monomers of wild-type and phosphomimetic versions of FUS 1-44 were solvated in a truncated octahedron box with 6.5 nm spaced faces (6742 and 6718 water molecules, respectively for wild type and phosphomimetic versions). Electrostatic interactions were calculated using the particle-mesh Ewald method (Essmann et al., 1995) with a real space cutoff distance of 0.9 nm. A 1.2 nm cutoff distance was used for the van der Waals interactions. Systems were propagated using stochastic Langevin dynamics with a friction coefficient of 1 ps^{-1}.

To analyze the NMR relaxation parameters from the simulation data, we also perform constant temperature molecular dynamics simulations of the wild type and phosphomimetic versions of FUS 1-44 monomers using the same run parameters as above (without enhanced sampling), also in NVT ensemble (T=300 K). 6 independent MD simulations are performed for each peptide using 6 randomly selected initial configurations from the equilibrium ensemble (see above). Each independent set is run for 220 ns, yielding a total of 1.32 μs simulation time per peptide. Results from dynamics trajectories are presented as averages over 6 independent simulations, and errors are the standard error calculated from the deviation between 6 simulations. For ^{15}N NMR relaxation rate constants calculations, N-H bond vector autocorrelation for each residue of each trajectory is extracted for the ensemble averaged second order Legendre polynomial autocorrelation function. Each autocorrelation decay curve is then fitted to a double exponential function such that

$C(t) = \sum_{i=1}^{n} a_i exp\,(\frac{-t}{\tau_i})$ satisfying $\sum_{i=1}^{n} a_i = 1$, where n=2 for our case.

Analytical Fourier transform of the autocorrelation function yields the spectral density function

$J(\omega) = \sum_{i=1}^{n} \frac{a_i \tau_i}{1+\omega^2 \tau_i^2}$.

^{15}N spin relaxation parameters are calculated as linear combinations of J(ω) sampled at the eigenfrequencies of the spin system:

$$R_1 = \frac{0.1\mu_0^2\gamma_{1H}^2\gamma_{15N}^2\hbar^2}{(4\pi)^2/r_{NH}^6}[J(\omega_{1H}-\omega_{15N})+3J(\omega_{15N})+6J(\omega_{1H}+\omega_{15N})] + \left(\frac{2}{15}\right)\omega_N^2(\sigma_\parallel-\sigma_\perp)^2[J(\omega_{15N})]$$

$$R_2 = \frac{0.05\mu_0^2\gamma_{1H}^2\gamma_{15N}^2\hbar^2}{(4\pi)^2/r_{NH}^6}[4J(0)+J(\omega_{1H}-\omega_{15N})+3J(\omega_{15N})+6J(\omega_{1H})+6J(\omega_{1H}+\omega_{15N})] + \left(\frac{1}{45}\right)\omega_N^2(\sigma_\parallel-\sigma_\perp)^2[3J(\omega_{15N})+4J(0)]$$

$$NOE = 1+\{\frac{0.1\mu_0^2\gamma_{1H}^3\gamma_{15N}\hbar^2}{(4\pi)^2/r_{NH}^6}[6J(\omega_{1H}+\omega_{15N})-J(\omega_{1H}-\omega_{15N})]\left(\frac{1}{R_1}\right)\}$$

.

In above equations, μ_0 is the permeability of free space, γ_i is gyromagnetic ratio of the spin i, $\hbar$ is reduced Planck's constant, $\sigma_\parallel$ and $\sigma_\perp$ are the parallel and perpendicular components of the axially symmetric ^{15}N chemical shift tensor, respectively. $\sigma_\parallel - \sigma_\perp$ is taken as -163 ppm (Yao et al., 2010), internuclear ^{1}H -^{15}N distance, r_{NH}, is taken as 1.02 Å and 850 MHz ^{1}H Larmor frequency is assumed in the calculation of R_1, R_2 and NOE.

Coarse grain simulations

Simulations were conducted in the LAMMPS software package (Plimpton, 1995, Plimpton et al., 2007) using an in-house developed coarse-grained model which utilizes the potential functional presented by Ashbaugh and Hatch (Ashbaugh & Hatch, 2008). Hydrophobic interactions between amino acid pairs were scaled according to Kapcha and Rossky's atomic-level hydrophobicity scale (Kapcha & Rossky, 2014). All systems consist of 22 chains of FUS, or one of its variants, and were equilibrated for a minimum of 1 microsecond each. Replica exchange molecular dynamics was used to improve sampling and to allow for exploration of temperature space.

Supplemental REFERENCES

Abascal JL, Vega C (2005) A general purpose model for the condensed phases of water: TIP4P/2005. J Chem Phys 123: 234505

Ashbaugh HS, Hatch HW (2008) Natively unfolded protein stability as a coil-to-globule transition in charge/hydropathy space. J Am Chem Soc 130: 9536-42

Berendsen HJC, Vanderspoel D, Vandrunen R (1995) Gromacs - a Message-Passing Parallel Molecular-Dynamics Implementation. Comput Phys Commun 91: 43-56

Best RB, Zheng W, Mittal J (2014) Balanced Protein-Water Interactions Improve Properties of Disordered Proteins and Non-Specific Protein Association. J Chem Theory Comput 10: 5113-5124

Bonomi M, Branduardi D, Bussi G, Camilloni C, Provasi D, Raiteri P, Donadio D, Marinelli F, Pietrucci F, Broglia RA, al. e (2009) PLUMED: A portable plugin for free-energy calculations with molecular dynamics. Comput Phys Commun 180: 1961-1972

Bonomi M, Parrinello M (2010) Enhanced sampling in the well-tempered ensemble. Phys Rev Lett 104: 190601

Bussi G, Gervasio FL, Laio A, Parrinello M (2006) Free-energy landscape for beta hairpin folding from combined parallel tempering and metadynamics. J Am Chem Soc 128: 13435-41

Deighan M, Bonomi M, Pfaendtner J (2012) Efficient Simulation of Explicitly Solvated Proteins in the Well-Tempered Ensemble. J Chem Theory Comput 8: 2189-92

Delaglio F, Grzesiek S, Vuister GW, Zhu G, Pfeifer J, Bax A (1995) NMRPipe: a multidimensional spectral processing system based on UNIX pipes. J Biomol NMR 6: 277-93

Edskes HK, Wickner RB (2000) A protein required for prion generation: [URE3] induction requires the Ras-regulated Mks1 protein. Proc Natl Acad Sci U S A 97: 6625-9

Edskes HK, Wickner RB (2002) Conservation of a portion of the S. cerevisiae Ure2p prion domain that interacts with the full-length protein. Proc Natl Acad Sci U S A 99 Suppl 4: 16384-91

Essmann U, Perera L, Berkowitz ML, Darden T, Lee H, Pedersen LG (1995) A Smooth Particle Mesh Ewald Method. Journal of Chemical Physics 103: 8577-8593

Farrow NA, Zhang O, Szabo A, Torchia DA, Kay LE (1995) Spectral density function mapping using 15N relaxation data exclusively. J Biomol NMR 6: 153-62

Fawzi NL, Ying J, Torchia DA, Clore GM (2010) Kinetics of amyloid beta monomer-to-oligomer exchange by NMR relaxation. J Am Chem Soc 132: 9948-51

Hess B, Kutzner C, van der Spoel D, Lindahl E (2008) GROMACS 4: Algorithms for Highly Efficient, Load-Balanced, and Scalable Molecular Simulation. J Chem Theory Comput 4: 435-47

Kapcha LH, Rossky PJ (2014) A simple atomic-level hydrophobicity scale reveals protein interfacial structure. J Mol Biol 426: 484-98

Masse JE, Keller R (2005) AutoLink: automated sequential resonance assignment of biopolymers from NMR data by relative-hypothesis-prioritization-based simulated logic. J Magn Reson 174: 133-51

Plimpton S (1995) Fast Parallel Algorithms for Short-Range Molecular-Dynamics. J Comput Phys 117: 1-19

Plimpton S, Crozier P, Thompson A (2007) LAMMPS-large-scale atomic/molecular massively parallel simulator. Sandia National Laboratories 18

Prakash MK, Barducci A, Parrinello M (2011) Replica Temperatures for Uniform Exchange and Efficient Roundtrip Times in Explicit Solvent Parallel Tempering Simulations. J Chem Theory Comput 7: 2025-7

Shen Y, Bax A (2010) SPARTA+: a modest improvement in empirical NMR chemical shift prediction by means of an artificial neural network. J Biomol NMR 48: 13-22

Sugita Y, Okamoto Y (1999) Replica-exchange molecular dynamics method for protein folding. Chem Phys Lett 314: 141-151

Sutto L, Gervasio FL (2013) Effects of oncogenic mutations on the conformational free-energy landscape of EGFR kinase. Proc Natl Acad Sci U S A 110: 10616-21

Thingholm TE, Jorgensen TJ, Jensen ON, Larsen MR (2006) Highly selective enrichment of phosphorylated peptides using titanium dioxide. Nat Protoc 1: 1929-35

Wilkins MR, Gasteiger E, Bairoch A, Sanchez JC, Williams KL, Appel RD, Hochstrasser DF (1999) Protein identification and analysis tools in the ExPASy server. Methods Mol Biol 112: 531-52

Yao L, Grishaev A, Cornilescu G, Bax A (2010) The impact of hydrogen bonding on amide 1H chemical shift anisotropy studied by cross-correlated relaxation and liquid crystal NMR spectroscopy. J Am Chem Soc 132: 10866-75